Rapid Communications

Tunable structural phase transition and superconductivity in the Weyl semimetal $Mo_{1-x}W_xTe_2$

R. Dahal,[1] L. Z. Deng,[1] N. Poudel,[2] M. Gooch,[1] Z. Wu,[1] H. C. Wu,[1,3] H. D. Yang,[3,4] C. K. Chang,[5] and C. W. Chu[1,6,*]

[1]*Texas Center for Superconductivity and Department of Physics, University of Houston, Houston, Texas 77204, USA*

[2]*Idaho National Laboratory, Idaho Falls, Idaho 83415, USA*

[3]*Department of Physics, National Sun Yat-sen University, Kaohsiung 80424, Taiwan*

[4]*Center of Crystal Research, National Sun Yat-sen University, Kaohsiung 80424, Taiwan*

[5]*National Synchrotron Radiation Research Center, Hsinchu 30076, Taiwan*

[6]*Lawrence Berkeley National Laboratory, 1 Cyclotron Road, Berkeley, California 94720, USA*

(Received 11 February 2020; accepted 25 March 2020; published 16 April 2020)

The relationship among structural transition, superconductivity, and doping in the Weyl semimetal $Mo_{1-x}W_xTe_2$ has been established through a systematic study of the doping and pressure effects. Doping-dependent resistivity measurements at ambient pressure revealed that the structural transition temperature increases linearly with increasing W content in $Mo_{1-x}W_xTe_2$. The observed structural transition temperature (T_s) of $MoTe_2$ at ambient pressure is 249 K and that of WTe_2 is 613 K. Temperature-dependent synchrotron x-ray diffraction measurements further confirmed the structural transition in WTe_2 at ambient pressure. Pressure was found to continuously suppress the T_s in $Mo_{0.90}W_{0.10}Te_2$, $Mo_{0.60}W_{0.40}Te_2$, and $Mo_{0.25}W_{0.75}Te_2$, and superconductivity emerges in $Mo_{0.90}W_{0.10}Te_2$ and $Mo_{0.60}W_{0.40}Te_2$ above 1.25 K when T_s is suppressed to a lower temperature.

DOI: 10.1103/PhysRevB.101.140505

Transition-metal dichalcogenides (TMDs) have been extensively investigated due to their wide-ranging electronic, optical, chemical, thermal, and mechanical properties, which are useful for device applications [1–7]. TMDs have a common formula MX_2, where M refers to a transition metal of group IVB (Ti, Zr, or Hf), VB (V, Nb, or Ta), or VIB (Cr, Mo, or W), and X is a chalcogen (S, Se, or Te) [8,9]. Most of the TMDs crystallize into a two-dimensional (2D) layered structure [10,11], in which each monolayer consists of transition-metal atoms between two planes of chalcogens (X-M-X). Atoms within a layer have a strong covalent bond, while interlayer bonding between the adjacent planes is by weak van der Waals–type forces. This feature gives rise to crystals that can be cleaved easily, and many of their physical properties are anisotropic [12]. TMDs can display semiconducting, semimetallic, or metallic behavior, which correlates well with the crystalline phase [13].

$MoTe_2$ and WTe_2 are both Weyl semimetals [14–17] with extremely large nonsaturating magnetoresistance (MR) and interesting physical properties [18,19]. The observed nonsaturating MR for $MoTe_2$ at 2 K and an applied field of 33 T is 61 700%, while that for WTe_2, 13 000 000% at 0.53 K and an applied field of 60 T, is even more impressive. When WTe_2 is thinned to a single monolayer, it becomes a 2D topological insulator with a conducting edge, in which a superconducting transition can be driven by applying a gate voltage [20,21]. Additionally, a dome-shaped superconducting behavior has been observed in both $MoTe_2$ and WTe_2 under pressure, with a maximum superconducting transition temperature (T_c) of 8.2 K at 11.7 GPa in $MoTe_2$ [22] and 7 K at 16.8 GPa in WTe_2 [23]. The Weyl semimetal state has also been observed in $Mo_{1-x}W_xTe_2$ for $x = 0.75$ and this compound has been predicted to be a tunable Weyl semimetal by varying x [24].

Depending on the synthesis conditions, $Mo_{1-x}W_xTe_2$ can crystallize into one of three different phases: the hexagonal 2H phase (space group $P6_3/mmc$), the monoclinic $1T'$ phase (space group $P2_1/m$), or the orthorhombic T_d phase (space group $Pmn2_1$) [10,25–28]. The $2H$ phase is semiconducting, whereas the $1T'$ and T_d phases are semimetallic. For $x \leqslant 0.10$, the compound is semiconducting at ambient conditions, while it is semimetallic above 900 °C, which can be stabilized at room temperature by rapid cooling. The compound is semimetallic for $x > 0.10$, independent of synthesis conditions. Rapid cooling of $MoTe_2$ results in the compound being in the $1T'$ phase at room temperature, whereas that of WTe_2 results in T_d phase. Thus, depending on the doping level in $Mo_{1-x}W_xTe_2$, the semimetallic phase can exhibit either $1T'$ or T_d structure at room temperature [27].

The semimetallic $1T'$-phase $MoTe_2$ undergoes a structural transition at ∼250 K to the T_d phase at ambient pressure [29,30]. External pressure suppresses the structural transition temperature (T_s) in $MoTe_2$ and, by suppressing the T_s to lower temperatures, the superconducting transition temperature (T_c) can be increased from 0.10 K at ambient pressure to 8.2 K at 11.7 GPa [22,31,32]. No structural transition in WTe_2 at ambient pressure has been reported to date. Kang *et al.* found no structural transition up to 20.1 GPa in WTe_2 by conducting synchrotron x-ray diffraction (XRD) at room temperature [33], while Zhuo *et al.* and Lu *et al.* both observed a room-temperature structural transition in WTe_2 starting under 6 and 4 GPa, respectively, by conducting synchrotron XRD [34,35]. Pressure is a basic and clean tuning parameter since it can have a great effect on physical and structural properties [31,36] by reducing atomic distances and shifting a

*Corresponding author: cwchu@uh.edu

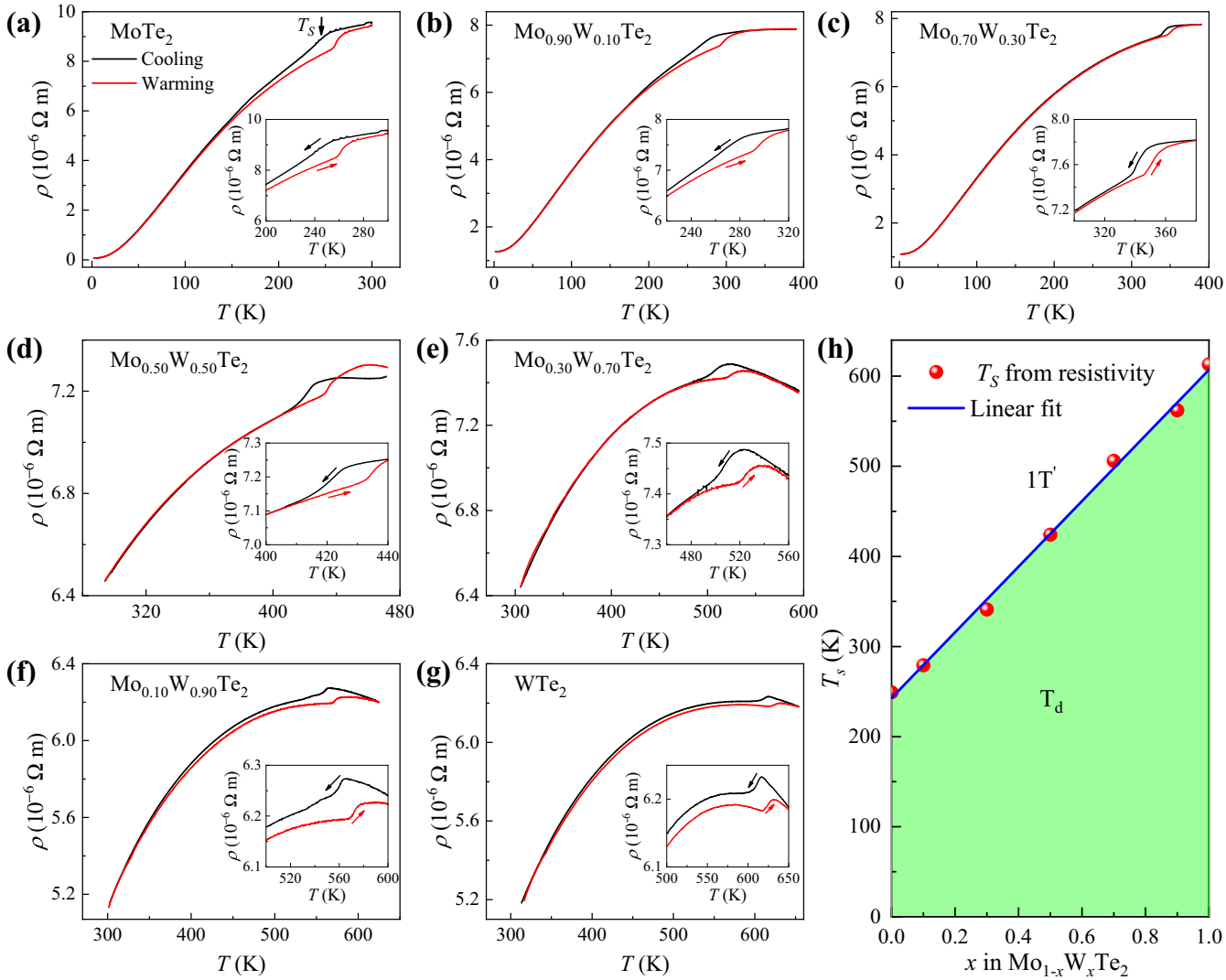

FIG. 1. Temperature-dependent resistivity of $Mo_{1-x}W_xTe_2$ in different temperature regions from 2 to 650 K for $x =$ (a) 0, (b) 0.10, (c) 0.30, (d) 0.50, (e) 0.70, (f) 0.90, and (g) 1, respectively. Insets to (a)–(g) show anomalies with thermal hysteresis associated with the structural transition from the monoclinic $1T'$ phase to the orthorhombic T_d phase. In (a)–(g), black curves correspond to the cooling cycles and red curves correspond to the warming cycles. (h) Variation of structural transition temperature T_s with doping in $Mo_{1-x}W_xTe_2$ obtained from resistivity measurements. T_s is taken at the maxima of $d\rho/dT$ during the cooling cycles.

compound's Fermi levels without complications arising from changing the chemistry of the compound. To explore the phase diagram of, and the effects of external pressure on, $Mo_{1-x}W_xTe_2$, we have conducted resistivity measurements on single crystals with selected doping levels under different pressures. The results show the relationship between T_s and W-doping x at ambient pressure and the suppression of T_s with increasing pressure, accompanied by the emergence of superconductivity.

Single crystals of $MoTe_2$ and WTe_2 were grown by the flux method described elsewhere [37,38]. Doped single crystals of $Mo_{1-x}W_xTe_2$ with nominal composition $x = 0.10$, 0.30, 0.40, 0.50, 0.70, 0.75, and 0.90 were prepared by the chemical vapor transport method using iodine as the transport agent following Ref. [27]. Synthesis details can be found in the Supplemental Material [39]. The compositions determined by energy-dispersive x-ray spectroscopy are shown in Table S1 in the Supplemental Material.

To investigate the relation between T_s and W concentration x, resistivity measurements up to 650 K were conducted for $x = 0$, 0.10, 0.30, 0.50, 0.70, 0.90, and 1, as shown in Figs. 1(a)–1(g). A clear hysteresis was observed in the resistivity for $MoTe_2$, which is associated with the first-order structural transition from the monoclinic $1T'$ phase to the orthorhombic T_d phase at $T_s = 249$ K, consistent with previous reports [11,22,29]. This anomaly was also observed for all other samples with different doping. The T_s's for the doped samples are 279, 341, 424, 506, 562, and 613 K for $x = 0.10$, 0.30, 0.50, 0.70, 0.90, and 1, respectively. T_s increases linearly with increasing x, as shown in Fig. 1(h). It has been reported that the $1T'$ phase has a slightly smaller equilibrium volume than the T_d phase in $MoTe_2$ [22]. Since W has a slightly larger atomic radius than Mo, an increase in x enlarges the equilibrium volume, the T_d phase with a larger equilibrium volume becomes energetically favorable, and more active energy is required to convert the T_d

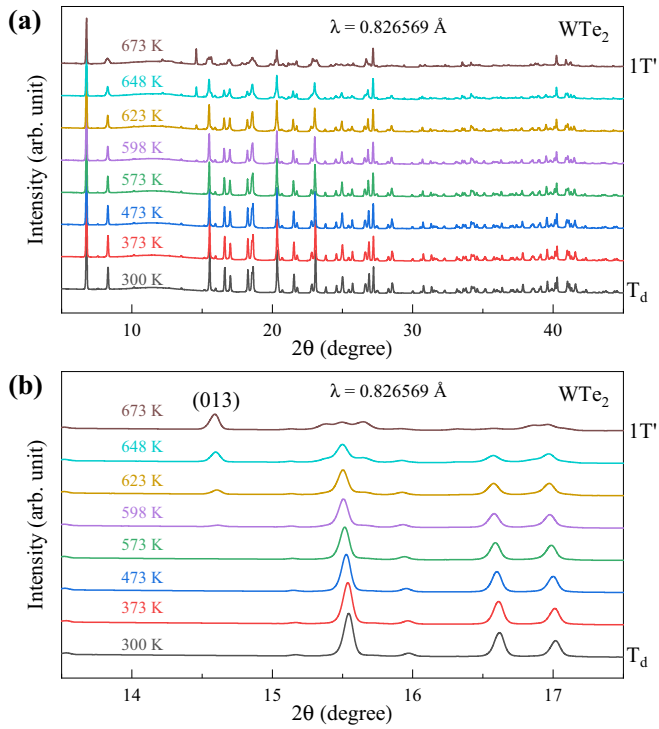

FIG. 2. Temperature-dependent synchrotron x-ray diffraction (XRD) patterns for WTe_2 (a) from 5° to 45° and (b) from 13.5° to 17.5°.

phase into the $1T'$ phase as mentioned in Ref. [28], leading to a higher T_s, which could explain the observed increase in T_s with increasing W concentration across the phase diagram.

In order to verify the structural transition and to obtain further structural information above T_s, WTe_2, which has the highest T_s, was selected for temperature-dependent synchrotron XRD measurements in the temperature range from 300 to 673 K. At 300 K, the orthorhombic T_d phase with the noncentrosymmetric space group $Pmn2_1$ is detected, as shown in Fig. 2(a), consistent with a previous report [26], and it persists up to 573 K. As the temperature increases to 598 K, a new Bragg reflection peak emerges, suggesting the breaking of the crystal symmetry. The new Bragg reflection peak was indexed as a 013 peak [Fig. 2(b)] with the monoclinic centrosymmetric $1T'$ phase ($P2_1/m$). As the temperature further increases, the intensity of the 013 peak increases as well, indicating the development of the $1T'$ phase. At 673 K the structure is completely transformed to the $1T'$ phase. Thus, the temperature-dependent synchrotron XRD results for WTe_2 are consistent with our resistivity measurement data.

To study the pressure effects on the doped compounds, single crystals with $x = 0.10,\ 0.40$, and 0.75 were investigated. At ambient pressure, $Mo_{0.90}W_{0.10}Te_2$ exhibits a ρ anomaly at T_s associated with the structural transition, as shown in Fig. 3(a). The ρ anomaly at T_s, characteristic of the $1T'$-to-T_d transition, diminishes with pressure up to 13.52 kbar and is no longer observable at 17.71 kbar (see Fig. S1 in

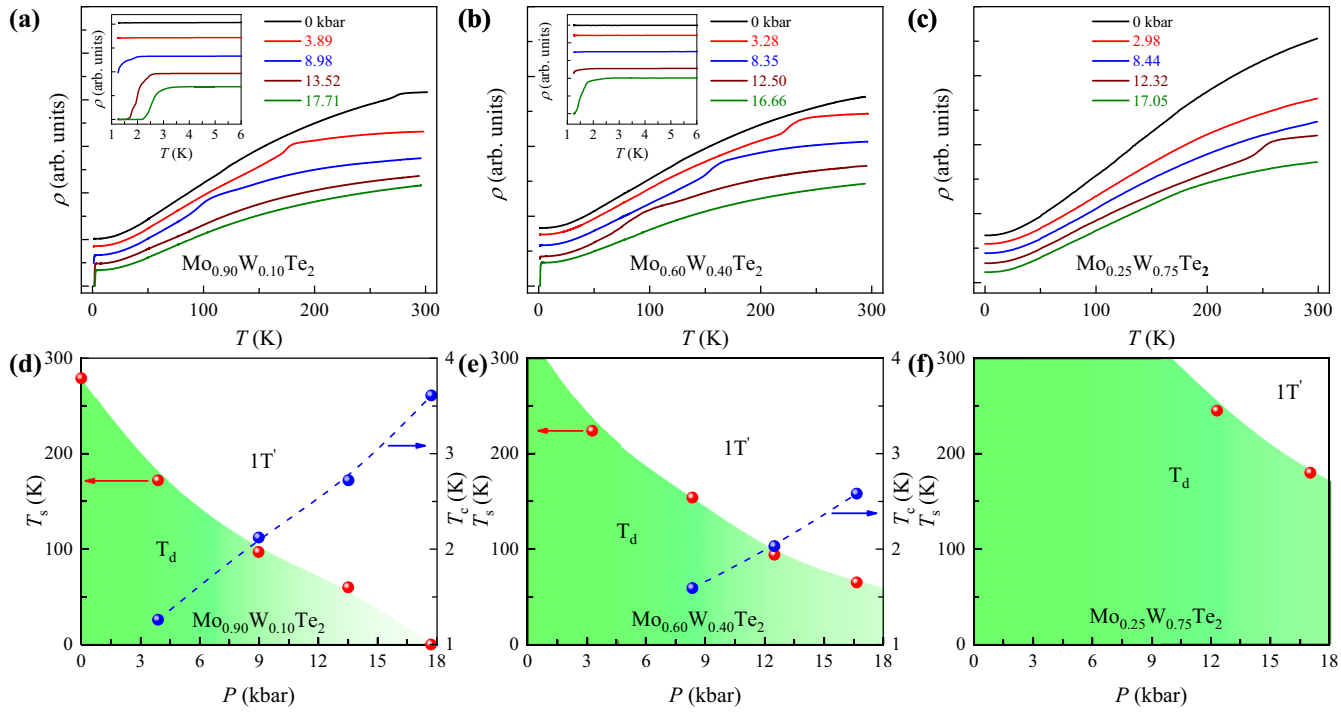

FIG. 3. Temperature-dependent resistivity of (a) $Mo_{0.90}W_{0.10}Te_2$, (b) $Mo_{0.60}W_{0.40}Te_2$, and (c) $Mo_{0.25}W_{0.75}Te_2$ at various pressures. For clarity, the resistivity curves have been shifted vertically. The anomaly in the resistivity corresponds to the structural transition from the monoclinic $1T'$ phase to the orthorhombic T_d phase. Insets to (a) and (b) show low-temperature-region data for $Mo_{0.90}W_{0.10}Te_2$ and $Mo_{0.60}W_{0.40}Te_2$, respectively. (d) and (e) Pressure-dependent structural transition (red spheres) and superconductivity (blue spheres) for $Mo_{0.90}W_{0.10}Te_2$ and $Mo_{0.60}W_{0.40}Te_2$, respectively. (f) Pressure-dependent structural transition for $Mo_{0.25}W_{0.75}Te_2$.

the Supplemental Material for hysteresis effects). A slight drop in ρ was observed at 3.89 kbar at 1.26 K. This ρ drop becomes more pronounced with increasing pressure and reaches zero at 13.52 kbar, which indicates the emergence of superconductivity at a transition temperature $T_c \sim 2.7$ K. With increasing pressure, the T_c continues to increase, and a T_c of 3.6 K is reached at 17.71 kbar.

No structural transition was detected for $Mo_{0.60}W_{0.40}Te_2$ at ambient pressure from room temperature down to 1.25 K, as shown in Fig. 3(b). However, a structural transition was observed at 244 K under 3.28 kbar, and T_s continuously decreases to ~65 K as pressure increases up to 16.66 kbar (see Fig. S2 in the Supplemental Material for hysteresis effects). Superconductivity was observed at 1.59 K around 8.35 kbar and T_c continuously increases to 2.6 K with further increasing pressure.

Initially, no ρ anomaly was observed in $Mo_{0.25}W_{0.75}Te_2$ at ambient pressure from room temperature down to 1.25 K, as shown in Fig. 3(c). However, as the pressure increases, the overall resistivity decreases, and at ~12.32 kbar a ρ anomaly with hysteresis (see Fig. S3 in the Supplemental Material), which is associated with a first-order structural transition [29], appears at 245 K. With further increasing pressure, the T_s is suppressed to around 180 K at 17.05 kbar, but superconductivity was not observed down to 1.25 K.

Temperature-pressure (T-P) phase diagrams for $x = 0.10$, $x = 0.40$, and $x = 0.75$ are shown in Figs. 3(d)–3(f), respectively. In all three compounds, increasing pressure continuously suppresses the T_s. We also found that pressures higher than 3.28 kbar are needed to suppress the T_s to below room temperature for $x \geqslant 0.40$. It has been reported that a structural transition in WTe_2 is observed at room temperature under pressures of 4–6 GPa [34,35]. In addition, pressure has also been found to suppress the T_s of $MoTe_2$ [31,32]. These observations support the existence of a structural transition in $Mo_{1-x}W_xTe_2$ at ambient pressure for all x, with higher T_s at higher W concentration. Among these three compounds, superconductivity was observed for $x = 0.10$ and $x = 0.40$. The T_c increases with pressure and the dT_c/dP is 0.17 K/kbar for $x = 0.10$ and 0.11 K/kbar for $x = 0.40$.

Competition between the structural transition and superconductivity in $Mo_{1-x}W_xTe_2$ is supported by the following observations. With increasing pressure, T_s continuously decreases, as shown in Figs. 3(d)–3(f). Once the T_s is suppressed to <175 K, superconductivity emerges (e.g., for $x = 0.10$ with a $T_c = 1.26$ K under 3.89 kbar and for $x = 0.40$ with a $T_c = 1.59$ K under 8.35 kbar). An increase in the T_c is coupled with the decrease of the T_s. Superconductivity was not observed for $x = 0.75$ down to 1.25 K with T_s down to ~180 K and under pressures up to 17 kbar. It has been previously reported that pressure continuously suppresses T_s in $MoTe_2$ [22,32,40] and that a sharp increase in T_c is observed in the pressure range from 2.7 to 7.5 kbar [31]. There have also been reports of pressure-induced structural transition in WTe_2 at room temperature [34,35]. However, our observation shows that WTe_2 has a structural transition at ambient pressure with $T_s = 613$ K; therefore, the previously reported structural transition under pressure in WTe_2 is more likely to be related to the suppression of the structural transition rather than being induced under pressure. Clarke *et al.* reported that although the structural transition in $MoTe_2$ at ambient pressure occurs around 250 K, two phases coexist in an extended temperature range from 233 to 290 K [30]. Heikes *et al.* have also shown that the $1T'$ and T_d phases co-exist in $MoTe_2$ at 1.5 K and under hydrostatic pressure of 1 GPa [32]. Once the T_s in $Mo_{1-x}W_xTe_2$ is suppressed by pressure to below critical temperature, completion of the structural transition occurs at very low temperature, after which the T_c sharply increases. These observations shed light on the possible origin(s) for the superconductivity in the $Mo_{1-x}W_xTe_2$ system, such as the competition between the superconductivity and the structural transition, and/or the coexistence of different phases.

Total energy calculations including the van der Waals interaction have shown that the T_d phase is energetically more stable than the $1T'$ phase [41]. The energy differences between the T_d and $1T'$ phases in $MoTe_2$ and WTe_2 are 0.40 and 0.46 meV per unit cell, respectively. This suggests that higher energy is required for the transition from the T_d phase to the $1T'$ phase in WTe_2 than in $MoTe_2$. It has been reported that the interlayer contraction increases the hybridization between the Te p_z orbitals, resulting in the enhancement of the three dimensionality of the band character [42]. Since the atomic radius of W is larger than that of Mo, an increase in W content expands the interlayer distance in $Mo_{1-x}W_xTe_2$ and reduces interlayer hybridization. Total kinetic energy of the electron increases as interlayer hybridization decreases [31]. The increase in kinetic energy leads to an increase in the total energy, assuming the rest changes negligibly. Thus, the energy difference between the T_d phase and the $1T'$ phase increases with increasing W composition. When the energy difference is larger, higher energy (and hence higher temperature) is required for the transition from the T_d phase to the $1T'$ phase, which explains the increasing T_s with increasing W content as shown in Fig. 1(h). On the other hand, the application of external pressure reduces the interlayer distance and enhances the interlayer hybridization, which leads to a lower T_s and favors superconductivity.

Applying pressure to $MoTe_2/WTe_2$ suppresses the interlayer Te-Te distances while the intralayer Mo-Te/W-Te [22,35] bond length is almost unchanged due to the anisotropy of the van der Waals structure. Lu *et al.* [35] pointed out that one transverse acoustic vibrational mode, mainly from Te-Te interlayer vibrations, contributes significantly to the electron-phonon coupling. It is thus natural to suggest that the pressure effect on $Mo_{1-x}W_xTe_2$ also leads to the softening of the interlayer Te-Te vibration modes. The superconducting transition temperature T_c can be estimated by the modified McMillan formula [43]:

$$T_c = \frac{\langle\omega\rangle}{1.20} \exp\Big(-\frac{1.04(1+\lambda)}{\lambda - \mu^*(1+0.62\lambda)}\Big), \quad (1)$$

where the parameter $\langle\omega\rangle$ is the average of phonon energy defined as $\langle\omega\rangle = \frac{2}{\lambda}\int_0^\infty d\omega\,\alpha^2F(\omega)$, μ^* is the Coulomb pseudopotential, and λ is the dimensionless electron-phonon coupling strength. λ in terms of the Eliashberg electron-phonon spectral function $\alpha^2F(\omega)$ is expressed as $\lambda = 2\int_0^\infty d\omega\,\alpha^2F(\omega)/\omega$, where α^2 is an average of the electron-phonon interaction, $F(\omega)$ is the phonon density of states, and ω is the phonon frequency. The phonon softening can result in an increase in the superconducting transi-

tion temperature, which could possibly be the origin of the emergence of superconductivity in $Mo_{1-x}W_xTe_2$ under high pressure.

In conclusion, the structural phase diagram of $Mo_{1-x}W_xTe_2$ at ambient pressure has been established. Resistivity measurements at ambient pressure and at temperatures up to 650 K have revealed some previously unreported structural phase transitions. T_s linearly increases with increasing W content from $MoTe_2$ to WTe_2, which is due to enhancement in the kinetic energy of the system with W doping. Additionally, the T-P phase diagrams of $Mo_{1-x}W_xTe_2$ for $x = 0.10$, $x = 0.40$, and $x = 0.75$ have been constructed. Based on our high-pressure resistivity measurements, we conclude that there is a competition between the structural transition and superconductivity in $Mo_{1-x}W_xTe_2$, in which superconductivity emerges when T_s is suppressed to <175 K and, as T_s is further suppressed, T_c increases.

The work in Houston is supported in part by U.S. Air Force Office of Scientific Research Grant No. FA9550-15-1-0236, the T. L. L. Temple Foundation, the John J. and Rebecca Moores Endowment, and the State of Texas through the Texas Center for Superconductivity at the University of Houston. N.P. acknowledges support from the Idaho National Laboratory's Laboratory Directed Research and Development program (18P37-008FP).

[1] J. A. Wilson and A. D. Yoffe, Adv. Phys. **18**, 193 (1969).
[2] Q. H. Wang, K. Kalantar-Zadeh, A. Kis, J. N. Coleman, and M. S. Strano, Nat. Nanotechnol. **7**, 699 (2012).
[3] A. D. Yoffe, Annu. Rev. Mater. Sci. **3**, 147 (1973).
[4] R. C. Morris, R. V. Coleman, and R. Bhandari, Phys. Rev. B **5**, 895 (1972).
[5] B. Sipos, A. F. Kusmartseva, A. Akrap, H. Berger, L. Forró, and E. Tutiš, Nat. Mater. **7**, 960 (2008).
[6] B. W. H. Baugher, H. O. H. Churchill, Y. Yang, and P. Jarillo-Herrero, Nat. Nanotechnol. **9**, 262 (2014).
[7] X. Qian, J. Liu, L. Fu, and J. Li, Science **346**, 1344 (2014).
[8] H. Katzke, P. Tolédano, and W. Depmeier, Phys. Rev. B **69**, 134111 (2004).
[9] A. R. Beal and H. P. Hughes, J. Phys. C: Solid State Phys. **12**, 881 (1979).
[10] B. E. Brown, Acta Crystallogr. **20**, 268 (1966).
[11] T. Zandt, H. Dwelk, C. Janowitz, and R. Manzki, J. Alloys Compd. **442**, 216 (2007).
[12] J. E. Callanan, G. Hope, R. D. Weir, and E. F. Westrum, J. Chem. Thermodyn. **24**, 627 (1992).
[13] F. Zhang, H. Zhang, S. Krylyuk, C. A. Milligan, Y. Zhu, D. Y. Zemlyanov, L. A. Bendersky, B. P. Burton, A. V. Davydov, and J. Appenzeller, Nat. Mater. **18**, 55 (2019).
[14] M. Sakano, M. S. Bahramy, H. Tsuji, I. Araya, K. Ikeura, H. Sakai, S. Ishiwata, K. Yaji, K. Kuroda, A. Harasawa, S. Shin, and K. Ishizaka, Phys. Rev. B **95**, 121101(R) (2017).
[15] J. Jiang, Z. K. Liu, Y. Sun, H. F. Yang, C. R. Rajamathi, Y. P. Qi, L. X. Yang, C. Chen, H. Peng, C. C. Hwang, S. Z. Sun, S.-K. Mo, I. Vobornik, J. Fujii, S. S. P. Parkin, C. Felser, B. H. Yan, and Y. L. Chen, Nat. Commun. **8**, 13973 (2017).
[16] Y.-Y. Lv, X. Li, B.-B. Zhang, W. Y. Deng, S.-H. Yao, Y. B. Chen, J. Zhou, S.-T. Zhang, M.-H. Lu, L. Zhang, M. Tian, L. Sheng, and Y.-F. Chen, Phys. Rev. Lett. **118**, 096603 (2017).
[17] P. Li, Y. Wen, X. He, Q. Zhang, C. Xia, Z.-M. Yu, S. A. Yang, Z. Zhu, H. N. Alshareef, and X.-X. Zhang, Nat. Commun. **8**, 2150 (2017).
[18] X. Luo, F. C. Chen, J. L. Zhang, Q. L. Pei, G. T. Lin, W. J. Lu, Y. Y. Han, C. Y. Xi, W. H. Song, and Y. P. Sun, Appl. Phys. Lett. **109**, 102601 (2016).
[19] M. N. Ali, J. Xiong, S. Flynn, J. Tao, Q. D. Gibson, L. M. Schoop, T. Liang, N. Haldolaarachchige, M. Hirschberger, N. P. Ong, and R. J. Cava, Nature (London) **514**, 205 (2014).
[20] Z. Fei, T. Palomaki, S. Wu, W. Zhao, X. Cai, B. Sun, P. Nguyen, J. Finney, X. Xu, and D. H. Cobden, Nat. Phys. **13**, 677 (2017).
[21] E. Sajadi, T. Palomaki, Z. Fei, W. Zhao, P. Bement, C. Olsen, S. Luescher, X. Xu, J. A. Folk, and D. H. Cobden, Science **362**, 922 (2018).
[22] Y. Qi, P. G. Naumov, M. N. Ali, C. R. Rajamathi, W. Schnelle, O. Barkalov, M. Hanfland, S.-C. Wu, C. Shekhar, Y. Sun, V. Süß, M. Schmidt, U. Schwarz, E. Pippel, P. Werner, R. Hillebrand, T. Förster, E. Kampert, S. Parkin, R. J. Cava, C. Felser, B. Yan, and S. A. Medvedev, Nat. Commun. **7**, 11038 (2016).
[23] X.-C. Pan, X. Chen, H. Liu, Y. Feng, Z. Wei, Y. Zhou, Z. Chi, L. Pi, F. Yen, F. Song, X. Wan, Z. Yang, B. Wang, G. Wang, and Y. Zhang, Nat. Commun. **6**, 7805 (2015).
[24] I. Belopolski, D. S. Sanchez, Y. Ishida, X. Pan, P. Yu, S.-Y. Xu, G. Chang, T.-R. Chang, H. Zheng, N. Alidoust, G. Bian, M. Neupane, S.-M. Huang, C.-C. Lee, Y. Song, H. Bu, G. Wang, S. Li, G. Eda, H.-T. Jeng, T. Kondo, H. Lin, Z. Liu, F. Song, S. Shin, and M. Z. Hasan, Nat. Commun. **7**, 13643 (2016).
[25] Y.-Y. Lv, L. Cao, X. Li, B.-B. Zhang, K. Wang, B. Pang, L. Ma, D. Lin, S.-H. Yao, J. Zhou, Y. B. Chen, S.-T. Dong, W. Liu, M.-H. Lu, Y. Chen, and Y.-F. Chen, Sci. Rep. **7**, 44587 (2017).
[26] W. G. Dawson and D. W. Bullett, J. Phys. C: Solid State Phys. **20**, 6159 (1987).
[27] S. M. Oliver, R. Beams, S. Krylyuk, I. Kalish, A. K. Singh, A. Bruma, F. Tavazza, J. Joshi, I. R. Stone, S. J. Stranick, A. V. Davydov, and P. M. Vora, 2D Mater. **4**, 045008 (2017).
[28] X.-J. Yan, Y.-Y. Lv, L. Li, X. Li, S.-H. Yao, Y.-B. Chen, X.-P. Liu, H. Lu, M.-H. Lu, and Y.-F. Chen, Appl. Phys. Lett. **110**, 211904 (2017).
[29] H. P. Hughes and R. H. Friend, J. Phys. C: Solid State Phys. **11**, L103 (1978).
[30] R. Clarke, E. Marseglia, and H. P. Hughes, Philos. Mag. B **38**, 121 (1978).
[31] H. Takahashi, T. Akiba, K. Imura, T. Shiino, K. Deguchi, N. K. Sato, H. Sakai, M. S. Bahramy, and S. Ishiwata, Phys. Rev. B **95**, 100501(R) (2017).
[32] C. Heikes, I-Lin Liu, T. Metz, C. Eckberg, P. Neves, Y. Wu, L. Hung, P. Piccoli, H. Cao, J. Leao, J. Paglione, T. Yildirim, N. P. Butch, and W. Ratcliff, II, Phys. Rev. Mater. **2**, 074202 (2018).
[33] D. Kang, Y. Zhou, W. Yi, C. Yang, J. Guo, Y. Shi, S. Zhang, Z. Wang, C. Zhang, S. Jiang, A. Li, K. Yang, Q. Wu, G. Zhang, L. Sun, and Z. Zhao, Nat. Commun. **6**, 7804 (2015).

[34] Y. Zhou, X. Chen, N. Li, R. Zhang, X. Wang, C. An, Y. Zhou, X. Pan, F. Song, B. Wang, W. Yang, Z. Yang, and Y. Zhang, AIP Adv. **6**, 075008 (2016).

[35] P. Lu, J.-S. Kim, J. Yang, H. Gao, J. Wu, D. Shao, B. Li, D. Zhou, J. Sun, D. Akinwande, D. Xing, and J.-F. Lin, Phys. Rev. B **94**, 224512 (2016).

[36] L. Z. Deng, Y. P. Zheng, Z. Wu, S. Huyan, H.-C. Wu, Y. F. Nie, K. Cho, and C.-W. Chu, Proc. Natl. Acad. Sci. U.S.A. **116**, 2004 (2019).

[37] J. Yang, J. Colen, J. Liu, M. C. Nguyen, G.-w. Chern, and D. Louca, Sci. Adv. **3**, eaao4949 (2017).

[38] E. J. Sie, C. M. Nyby, C. D. Pemmaraju, S. J. Park, X. Shen, J. Yang, M. C. Hoffmann, B. K. Ofori-Okai, R. Li, A. H. Reid, S. Weathersby, E. Mannebach, N. Finney, D. Rhodes, D. Chenet, A. Antony, L. Balicas, J. Hone, T. P. Devereaux, T. F. Heinz, X. Wang, and A. M. Lindenberg, Nature (London) **565**, 61 (2019).

[39] See Supplemental Material at http://link.aps.org/supplemental/10.1103/PhysRevB.101.140505 for experimental methods.

[40] Y. J. Hu, Y. T. Chan, K. T. Lai, K. O. Ho, X. Guo, H.-P. Sun, K. Y. Yip, D. H. L. Ng, H.-Z. Lu, and S. K. Goh, Phys. Rev. Mater. **3**, 034201 (2019).

[41] H.-J. Kim, S.-H. Kang, I. Hamada, and Y.-W. Son, Phys. Rev. B **95**, 180101(R) (2017).

[42] K. Ikeura, H. Sakai, M. S. Bahramy, and S. Ishiwata, APL Mater. **3**, 041514 (2015).

[43] R. C. Dynes, Solid State Commun. **10**, 615 (1972).